Promoter-Induced Nonlinear Pattern Formation in Surface Chemical Reactions†

ARTICLE *in* THE JOURNAL OF PHYSICAL CHEMISTRY B · JULY 2004

Impact Factor: 3.3 · DOI: 10.1021/jp0485587

2 AUTHORS, INCLUDING:

Alexander S. Mikhailov
Fritz Haber Institute of the Max Planck Society
285 PUBLICATIONS **6,220** CITATIONS

SEE PROFILE

Promoter-Induced Nonlinear Pattern Formation in Surface Chemical Reactions†

Yannick De Decker‡ and Alexander S. Mikhailov*,§

Center for Nonlinear Phenomena and Complex Systems, Université Libre de Bruxelles, Campus Plaine, C.P. 231. B-1050 Brussels, Belgium, and Abteilung Physikalische Chemie, Fritz-Haber-Institut der Max-Planck-Gesellschaft, Faradayweg 4-6, 14195 Berlin, Germany

Received: April 2, 2004

A simple model of a surface chemical reaction with a promoter interacting with one of the reactants is considered. We show that an interplay between the reaction, interactions, and diffusion of species in this system can result in the development of periodic nonequilibrium spatial patterns. The instability leading to such patterns is analyzed, and numerical investigations of nonlinear pattern formation are performed.

I. Introduction

Already the first spatially resolved observations of surface chemical reactions by electron microscopy have shown that such reactions are accompanied by rich phenomena of nonlinear pattern formation, including traveling waves, rotating spirals, pacemakers, and chemical turbulence.[1] Today, studies of reaction-induced patterns in heterogeneous catalysis represent an integral part of nonlinear science.[2] Promoters and poisons are adsorbed chemical species, often ions of alkali metals, that enhance or slow a surface reaction without being consumed in it.[3,4] Recent experiments indicate that such species can have a strong effect on nonlinear pattern formation. In the $O_2 + H_2$ reaction on the Rh(110) surface in the presence of coadsorbed potassium, it was observed that potassium ions were not uniformly distributed over the surface and that large K + O islands were formed.[5−7] Under different conditions, spontaneous formation of periodic stationary patterns with a definite wavelength was observed and investigated in this system by using photoemission electron microscopy (PEEM) and scanning photoelectrom microscopy (SPEM).[8] A typical property of promoter ions is that they are mobile and have a high affinity to one of the reactants. According to a general analysis of reactive systems with interactions between molecules, an interplay between reaction, diffusion, and attractive interactions can lead to the development of waves and nonequilibrium stationary patterns on the length scales significantly shorter than the diffusion length of involved reactants.[9] Indeed, chemical reactions in phase-separating polymer mixtures are known to induce nonequilibrium periodic stationary patterns,[10−12] and self-organized traveling waves were observed in illuminated Langmuir monolayers.[13,14] Similar phenomena are possible in surface chemical reactions where reaction-induced stationary and traveling nanostructures have previously been theoretically demonstrated.[15−18] Their theoretical description is based on mesoscopic kinetic equations for surface chemical reactions with energetic interactions between adsorbed molecules. Such mesoscopic equations have first been phenomenologically constructed[19] and then analytically derived by coarse graining of the master equation;[20,21] they were subsequently verified by comparing their predictions with kinetic Monte Carlo simulations.[22,23]

As a step toward a study of nonlinear pattern formation in surface reactions with promoters, we consider here a simple hypothetical model (see also ref 8). Two reactants arrive by adsorption onto the catalytic surface, diffuse on it, react, and form a product that immediately desorbs. We show that introduction of a promoter species, attracting one of the reactants, shall usually lead to an instability of the uniform state in this system and to spontaneous development of periodic spatial concentration patterns. The patterns represent the periodic array of small islands (dots) where local coverages of the promoter and one of the reactants are increased. When interactions are sufficiently strong, the reaction becomes confined to such dots playing a role of microreactors. Effective compartmentalization of the system leads to an increase of the reaction rate, thus enhancing the promoter effect. In the framework of this model, systems with repulsion between promoters and reactants and systems with poisons are also considered. In section II, the model is described and mesoscopic kinetic evolution equations are constructed. The stability analysis of the uniform state is performed in the next section. Section IV presents numerical simulations of nonlinear pattern formation in the considered system. The paper ends with the discussion of obtained results.

II. The Model and Its Kinetic Equations

We consider an abstract reaction scheme where molecules A and B adsorb from the gas phase and react on the surface

$$\mathrm{A} + *_{\mathrm{A}} \rightarrow \mathrm{A}_{\mathrm{ad}}$$

$$\mathrm{B} + *_{\mathrm{B}} \rightarrow \mathrm{B}_{\mathrm{ad}}$$

$$\mathrm{A}_{\mathrm{ad}} + \mathrm{B}_{\mathrm{ad}} \rightarrow *_{\mathrm{A}} + *_{\mathrm{B}} + \mathrm{P} \qquad (1)$$

Here $*_A$ and $*_B$ denote vacant surface sites for molecules A and B (they are different for the two reactants). The product *P* immediately leaves the surface. Surface diffusion of adsorbed molecules A_{ad} and B_{ad} is characterized by diffusion constants D_A and D_B. The reaction rate constant is k_r, the sticking coefficients of both reactants are k_{ads}^{A} and k_{ads}^{B}, and their partial pressures in the gas phase are p_A and p_B.

† Part of the special issue "Gerhard Ertl Festschrift".

* To whom correspondence may be addressed. E-mail: mikhailov@fhi-berlin.mpg.de.

‡ Université Libre de Bruxelles.

§ Fritz-Haber-Institut der Max-Planck-Gesellschaft.

10.1021/jp0485587 CCC: $27.50
Published on Web 07/22/2004

Mobile promoter C is present on the surface. Diffusion constant of this adsorbed species is D_C. In our phenomenological model, we do not explicitly consider the microscopic mechanisms, responsible for the promoter effect (see, e.g., ref 24), and take it into account by postulating an Arrhenius dependence of the reaction rate constant on the local promoter coverage θ_C

$$\nu(\mathbf{r}) = \nu_0 \exp[\rho\theta_C(\mathbf{r})/k_B T] \tag{2}$$

where ν_0 is the reaction rate constant in absence of the promoter, T is the temperature, and the coefficient ρ specifies how strongly the reaction is affected by the promoter. Note that if this coefficient is negative, the species C slows down the local reaction and therefore actually represents a poison.

Energetic lateral interactions between promoter C and the reactant A are present. In real systems, such lateral interactions are typically mediated through the metal substrate and can extend up to several lattice lengths; their dependence on the separation between the particles should be determined by the microscopic analysis of a particular system. In the model, we choose a Gaussian binary interaction potential

$$u_{AC}(\mathbf{r}-\mathbf{r}') = \frac{u_0}{(\pi r_0^{\,2})^{d/2}} \exp\left(-\frac{|\mathbf{r}-\mathbf{r}'|^2}{r_0^{\,2}}\right) \tag{3}$$

where r_0 is the characteristic interaction radius and the coefficient u_0 specifies the interaction strength. Positive values of u_0 correspond to attraction and negative values to repulsion between the considered particles. The parameter $d = 1$ and 2 is the medium dimensionality (some numerical simulations shall be performed for a one-dimensional system).

To describe pattern formation in this system, we need mesoscopic kinetic equations that would take into account interactions between adsorbed particles and describe processes of phase separation. Such equations are obtained by applying coarse graining to the stochastic master equation of the system (see refs 20−23). The surface is divided into boxes of size l^d centered at positions $\mathbf{r}$. Inside each of these boxes, the total number of particles must be large enough to ensure that the relevant thermodynamic quantities, such as the local free energy, can be defined at any moment t and that fluctuations may be neglected. On the other hand, this number must also be small enough so that these quantities can be considered as constant within each box, and so that the rules of differential analysis can be applied. Moreover, we shall assume that the conditions of local equilibrium hold, i.e., inside each cell the thermodynamic potentials have the same form as in equilibrium, but with varying state variables.

In this approximation, the free-energy density is given by a difference $f(\mathbf{r}) = u(\mathbf{r}) - Ts(\mathbf{r})$, where $u(\mathbf{r})$ is the local internal energy and $s(\mathbf{r})$ is the local entropy density, so that

$$\begin{aligned} f(\mathbf{r}) = {} & -\theta_A(\mathbf{r}) \int d\mathbf{r}' u_{AC}(\mathbf{r}-\mathbf{r}')\theta_C(\mathbf{r}') - \\ & \theta_C(\mathbf{r}) \int d\mathbf{r}' u_{AC}(\mathbf{r}-\mathbf{r}')\theta_A(\mathbf{r}') + k_B T[\theta_A(\mathbf{r}) \ln \theta_A(\mathbf{r}) + \\ & (1-\theta_A(\mathbf{r})) \ln(1-\theta_A(\mathbf{r})) + \theta_B(\mathbf{r}) \ln \theta_B(\mathbf{r}) + \\ & (1-\theta_B(\mathbf{r})) \ln(1-\theta_B(\mathbf{r})) + \theta_C(\mathbf{r}) \ln \theta_C(\mathbf{r}) + \\ & (1-\theta_C(\mathbf{r})) \ln (1-\theta_C(\mathbf{r}))] \end{aligned} \tag{4}$$

Here, the last term corresponds to the free energy of the two-dimensional lattice gases A, B, and C. Thus, the following chemical potentials are derived

$$\mu_A(\mathbf{r}) = -\int d\mathbf{r}' u_{AC}(\mathbf{r}'-\mathbf{r})\theta_C(\mathbf{r}') + k_B T \ln\left(\frac{\theta_A(\mathbf{r})}{1-\theta_A(\mathbf{r})}\right) \equiv U(\mathbf{r}) + k_B T \ln\left(\frac{\theta_A(\mathbf{r})}{1-\theta_A(\mathbf{r})}\right) \tag{5}$$

$$\mu_B(\mathbf{r}) = k_B T \ln\left(\frac{\theta_B(\mathbf{r})}{1-\theta_B(\mathbf{r})}\right) \tag{6}$$

$$\mu_C(\mathbf{r}) = -\int d\mathbf{r}' u_{AC}(\mathbf{r}'-\mathbf{r})\theta_A(\mathbf{r}') + k_B T \ln\left(\frac{\theta_C(\mathbf{r})}{1-\theta_C(\mathbf{r})}\right) \equiv V(\mathbf{r}) + k_B T \ln\left(\frac{\theta_C(\mathbf{r})}{1-\theta_C(\mathbf{r})}\right) \tag{7}$$

By use of these potentials, one can easily obtain evolution equations for different coverages.

For deriving the diffusion terms, we assume that the transport process is not too far from equilibrium, so that the diffusion flux depends linearly on the corresponding driving force

$$J_A^{diff} = -L_{AA}\nabla\mu_A(\mathbf{r}) = -L_{AA}\left[\nabla U(\mathbf{r}) + \frac{k_B T}{\theta_A(\mathbf{r})(1-\theta_A(\mathbf{r}))}\nabla\theta_A(\mathbf{r})\right] \tag{8}$$

In absence of lateral interactions, one has to recover the classical Fick law, indicating that the phenomenological coefficient L_{AA} should be given by the relation

$$L_{AA} = \frac{D_A \theta_A(\mathbf{r})(1-\theta_A(\mathbf{r}))}{k_B T} \tag{9}$$

Replacing L_{AA} by this expression, we finally obtain

$$J_A^{diff} = -D_A\nabla\theta_A(\mathbf{r}) - \frac{D_A}{k_B T}\theta_A(\mathbf{r})(1-\theta_A(\mathbf{r}))\nabla U(\mathbf{r}) \tag{10}$$

The nonFickian term of this diffusion flux describes the viscous surface flow of the adsorbate A in the presence of a force induced by a surface gradient of the promoter coverage C. The factor $\theta_A(\mathbf{r})(1-\theta_A(\mathbf{r}))$ is representative of the fact that the flow of particles A can only pass through the empty sites on the surface. The same procedure can be applied to determine the diffusion flux of the promoter C, yielding

$$J_C^{diff} = -D_C\nabla\theta_C(\mathbf{r}) - \frac{D_C}{k_B T}\theta_C(\mathbf{r})(1-\theta_C(\mathbf{r}))\nabla V(\mathbf{r}) \tag{11}$$

The diffusion of the reactant B is not influenced by interactions, and its diffusion flux is

$$J_B^{diff} = -D_B\nabla\theta_B(\mathbf{r}) \tag{12}$$

Generally, the diffusion coefficients D_A, D_B, and D_C can still depend on the coverages, but we neglect such dependences in the considered simple model.

Note that eq 10 has first been proposed based on phenomenological arguments[19] and later derived by coarse graining starting from a Glauber-type master equation.[20,21] The validity of the respective mesoscopic approximation has been verified by comparing its predictions with the data of kinetic Monte Carlo simulations.[22,23]

Substituting explicit integral expressions for the potentials U and V and using new notations $P_A = k_{ads}^A p_A$, $P_B = k_{ads}^B p_B$, $\epsilon = u_0/k_BT$, and $w = \rho/k_BT$, the following set of mescopic kinetic equations is obtained

$$\dot{\theta}_A = P_A(1-\theta_A) - \nu_0\, e^{w\theta_c}\,\theta_A\theta_B + D_A\nabla^2\theta_A - \epsilon D_A\nabla\left[\theta_A(1-\theta_A)\nabla\int \frac{d\mathbf{r}'}{[r_0^{\,2}\pi]^{d/2}}\exp\left(-\frac{(\mathbf{r}-\mathbf{r}')^2}{r_0^{\,2}}\right)\theta_C(\mathbf{r}')\right] \quad (13)$$

$$\dot{\theta}_B = P_B(1-\theta_B) - \nu_0\, e^{w\theta_c}\,\theta_A\theta_B + D_B\nabla^2\theta_B \quad (14)$$

$$\dot{\theta}_C = D_C\nabla^2\theta_C - \epsilon D_C\nabla\left[\theta_C(1-\theta_C)\nabla\int \frac{d\mathbf{r}'}{[r_0^{\,2}\pi]^{d/2}}\exp\left(-\frac{(\mathbf{r}-\mathbf{r}')^2}{r_0^{\,2}}\right)\theta_A(\mathbf{r}')\right] \quad (15)$$

In addition to adsorption, reaction, and diffusion terms, they include also the terms that describe viscous surface flows of the adsorbates A and C. These flows are induced by the lateral forces which act on these adsorbates and are due to the potential gradients.

In the employed notations, the positive sign of ϵ corresponds to attractive interaction between A and C and the negative sign corresponds to repulsion between them. When w is positive, the species C is a promoter, whereas for $w < 0$, it represents a poison. The interaction radius r_0 is very short and can be used as a small parameter in the approximate theory. The model has previously been briefly presented in ref 8.

III. Instability of the Uniform State

In this section, we consider the instability of the uniform state of the system with respect to growth of periodic spatial modes. Our analysis is carried out only in the special case $w = 0$, when the species C has no direct effect on the reaction rate. As evidenced by numerical simulations that shall be presented in the next section, its results remain however to be qualitatively valid also for the general case with $w \neq 0$.

The considered kinetic model (eqs 13−15) has a uniform stationary state where all coverages are constant: $\theta_A(\mathbf{r}) \equiv a$, $\theta_B(\mathbf{r}) \equiv b$, and $\theta_C(\mathbf{r}) \equiv c$. Because the promoter C does not desorb and is not consumed in the reaction, its coverage c in the uniform state is determined by the initial conditions and represents a parameter of the system. The coverages a and b of both reactants in the uniform reactive state are yielded by a balance between adsorption and reaction, and are given by

$$a = \frac{P_A}{P_A + \nu_0 b} \quad (16)$$

$$b = -\frac{P_AP_B + \nu_0(P_A - P_B)}{2\nu_0P_B} + \frac{[(P_AP_B + \nu(P_A - P_B))^2 + 4\nu_0P_AP_B^{\,2}]^{1/2}}{2\nu_0P_B} \quad (17)$$

Note that this uniform state is always unique and that bistability never occurs in the system.

Because of the energetic interactions between adsorbed molecules A and C, diffusion of adsorbed species, and the chemical reaction, the uniform stationary state of the system can become unstable with respect to growth of nonuniform perturbations, signaling the development of a nonuniform spatial pattern. The initial stage of growth of such perturbations can be investigated by using a linearized version of the full kinetic model. To investigate the stability of the uniform state (a, b, and c), we introduce small perturbations of variables and linearize eqs 13−15. Solutions of the linearized equations can be sought in the form $\theta_A(\mathbf{r},t) = a + \delta\theta_A\, e^{i\mathbf{k}\mathbf{r}+\gamma_k t}$, $\theta_B(\mathbf{r},t) = b + \delta\theta_B\, e^{i\mathbf{k}\mathbf{r}+\gamma_k t}$, and $\theta_C(\mathbf{r},t) = c + \delta\theta_C\, e^{i\mathbf{k}\mathbf{r}+\gamma_k t}$. Each perturbation mode with a certain wavenumber k is characterized by its growth (or decay) rate γ_k. The growth rates of various modes are given by the eigenvalues of the linearization matrix

$$\mathcal{A}(k) = \begin{pmatrix} -P_A - \nu_0 b - D_Ak^2 & -\nu_0 a & -\epsilon D_Ak^2a(1-a)\, e^{(-r_0^2k^2/4)} \\ -\nu_0 b & -P_B - \nu_0 a - D_Bk^2 & 0 \\ -\epsilon D_Ck^2c(1-c)\, e^{(-r_0^2k^2/4)} & 0 & -D_Ck^2 \end{pmatrix} \quad (18)$$

or, explicitly, as the roots of the cubic equation

$$\gamma_k^{\,3} + \mathcal{A}\gamma_k^{\,2} + \mathcal{B}\gamma_k + \mathcal{C} = 0 \quad (19)$$

where the coefficients are defined as

$$\mathcal{A} = -\mathrm{Tr}(\mathcal{A}(k)) \quad \mathcal{B} = \sum_{i=1}^{3}\Delta_i^{(2)}(k) \quad \mathcal{C} = -\det(\mathcal{A}(k)) \quad (20)$$

and $\Delta_i^{(2)}(k)$ are the principal minors of the matrix $\mathcal{A}(k)$.

The uniform state of the system is stable if any perturbation mode is decaying with time, i.e., $\mathrm{Re}\gamma_k < 0$ for any k. The instability of the uniform state is found when one of the modes with a certain wavenumber $k = k_c$ begins to grow. Numerical investigations of the considered model show that it does not exhibit oscillations and therefore, when an instability of the uniform state occurs, it corresponds to a mode with a purely real γ_k. The instability boundary is thus determined by the condition that

$$\gamma_k = \frac{d\gamma_k}{dk} = 0 \quad \text{for} \quad k = k_c \quad (21)$$

and that all other modes are characterized by $\gamma_k < 0$ on the instability boundary.

Because $\mathcal{C}$ is equal to the product of all three roots of the cubic eq 19, if one of them is zero, the same is true for $\mathcal{C}$. Thus, on the instability boundary we have $\mathcal{C} = 0$. Moreover, if the derivative of the vanishing root with respect to k is zero, the same should hold for the coefficient $\mathcal{C}$. Thus, the instability boundary is determined by two conditions

$$\mathcal{C}(k_c^{\,2}) = \left(\frac{d\mathcal{C}}{dk^2}\right)_{k_c^2} = 0 \quad (22)$$

By computing the determinant of the linearization matrix and making use of these two conditions, the following two equations are obtained (we assume $k_c \neq 0$)

$$D_AD_B(1-\beta_k)k_c^{\,4} + [\sigma - D_A(P_B + \nu_0 a)\beta_k]k_c^{\,2} + \mu = 0 \quad (23)$$

$$\frac{1}{2} r_0^2 D_A D_B \beta_k k_c^6 + \left[\frac{1}{2} r_0^2 D_A (P_B + \nu_0 a)\beta_k + 3 D_A D_B (1 - \beta_k)\right] k_c^4 + 2[\sigma - 2D_A (P_B + \nu_0 a)\beta_k] k_c^2 + \mu = 0 \quad (24)$$

Here, new notations have been introduced

$$\beta_k = \epsilon^2 a(1-a)c(1-c)\, e^{-r_0^2 k_c^2/2} \quad (25)$$

$$\mu = P_A \nu_0 a + P_B \nu_0 b + P_A P_B$$

$$\sigma = P_A D_B + \nu_0 b D_B + P_B D_A + \nu_0 a D_A$$

To solve eq 22, we express β_k from the first of them

$$\beta_k = \frac{D_A D_B k_c^4 + \sigma k_c^2 + \mu}{D_A D_B k_c^4 + D_A (P_B + \nu_0 a) k_c^2} \quad (26)$$

Substituting this into eq 23, a quartic equation for k_c^2 is derived

$$D_A D_B^2 r_0^2 k_c^8 + D_B r_0^2 [(P_B + a) D_A + \sigma] k_c^6 + [2(P_B + \nu_0 a) D_A D_B - 2 D_B \sigma + (P_B + \nu_0 a) r_0^2 \sigma + D_B \mu r_0^2] k_c^4 - [4 D_B \mu - (P_B + \nu_0 a) r_0^2 \mu] k_c^2 - 2(P_B + \nu_0 a)\mu = 0 \quad (27)$$

To analytically find an approximate solution, we take further into account that the interaction radius r_0 is very small. Keeping only the leading terms, eq 27 can be easily solved. Thus, the wavenumber of the critical mode is determined

$$k_c^2 = \frac{1}{r_0}\left[\frac{2(P_A + \nu_0 b)}{D_A}\right]^{1/2} \quad (28)$$

Substituting this into eq 26, using the definition of β_k and keeping again only the leading term in the interaction radius r_0, we find that the instability boundary is approximately determined by the condition

$$\epsilon_c^2 = \frac{1}{a(1-a)c(1-c)} \quad (29)$$

Analyzing these results, we notice that the instability boundary (eq 29) is effectively the same as the boundary for spinodal decomposition in the mixture of two species A and C with surface coverages a and c in absence of reaction. Only the square of ϵ enters into the condition (eq 29), and therefore, the instability is found both for the attraction ($\epsilon > 0$) and repulsion ($\epsilon < 0$) between species A and C.

Equation 28 shows that the wavenumber of the critical mode does not depend on the diffusion constant D_C of the species C. This result is general and is not sensitive to a particular approximation. Indeed, the critical mode has marginal stability ($\gamma_k = 0$) and should therefore satisfy the evolution eq 15 with $\dot{\theta}_C = 0$. But stationary solutions of this equation, as can be easily seen, are independent of the diffusion constant D_C. We also note that the critical wavenumber does not depend on the diffusion constant D_B of the second reactant. This result is approximate and holds only in the limit of a very small interaction radius r_0.

IV. Numerical Investigations

Numerical simulations of eqs 13−15 have been undertaken in order to verify the predictions of the linear stability analysis and to study the nonlinear behavior of the system. These simulations were performed by using an explicit forward-time centered-space finite-difference scheme. The spatial step was fixed at $\Delta x = 0.01$, and the temporal step Δt was chosen differently in each particular simulation, in such a way that the numerical stability condition $D\Delta t \le \Delta x^2/4$ was satisfied for the maximum diffusion constant $D = \max(D_A, D_B, D_C)$. Because of a rapid exponential decrease of the interaction potential, to speed up numerical simulations, the interaction function (eq 3) was truncated at distances exceeding $2r_0/\Delta x$. Periodic boundary conditions were used. As initial conditions, the unstable stationary uniform state of the system $\theta_A = a$, $\theta_B = b$, and $\theta_C = c$ with small local random perturbations of about one percent in magnitude was always chosen. Since adsorption and desorbtion of C is absent and this species is not consumed in the reaction, its total coverage is conserved and c represents a system parameter determining the amount of species C present on the surface.

Figure 1. Space−time diagram showing the development of a periodic spatial pattern. Time runs along the horizontal axis, and the spatial coordinate is plotted along the vertical axis. The size of the one-dimensional system is $L = 20$, and the displayed time interval is $T = 50$. Local concentration of species C is displayed in gray scale, with brighter areas corresponding to higher concentrations. The model parameters are $P_A = P_B = D_A = D_B = D_C = 1$, $c = 0.5$, $\epsilon = 5$, $r_0 = 0.2$, and $w = 0$.

Numerical simulations for the case $w = 0$, considered in the previous section, will be first presented. Figure 1 shows an example of an evolution starting with a randomly performed uniform state. In this space-time diagram, time runs along the horizontal axis and the spatial coordinate of the simulated one-dimensional system is varied along the vertical axis. The local promoter coverage is displayed in gray scale, with bright areas corresponding to high surface concentrations. We see that the uniform state is indeed unstable, and a stationary periodic pattern develops, as predicted by the previous linear stability analysis.

Detailed numerical investigations of nonlinear periodic patterns, emerging as a result of the instability of the uniform state, have been performed. Figure 2a displays profiles of all three coverages in such a pattern in the case of attractive interactions, with the parameters lying close to the instability boundary. The amplitudes of spatial variation are relatively small here, and the pattern is approximately harmonical. The local coverage of the reactant A follows the variation of the surface concentration of species C; the coverage of reactant B exhibits weak antiphase variation. In Figure 2b, the interaction strength is increased to $\epsilon = 20$, as compared with $\epsilon = 5$ in Figure 2a. Now, the concentration profiles are strongly unharmonical and a periodic pattern of domains is clearly observed. Inside each domain, the coverage of species C reaches its maximum possible level of unity. Outside of the domains, almost no species C is found. The domains have sharp interfaces. The surface concentration of the reactant A, attracted by the species C, is strongly increased inside the domains and is very low outside of them. It can be noticed that the domains, formed by the reactant, are slightly larger than the respective distributions for the species C.

Nonlinear pattern formation in the two-dimensional system is illustrated in Figure 3. Here, the same parameters as in Figure

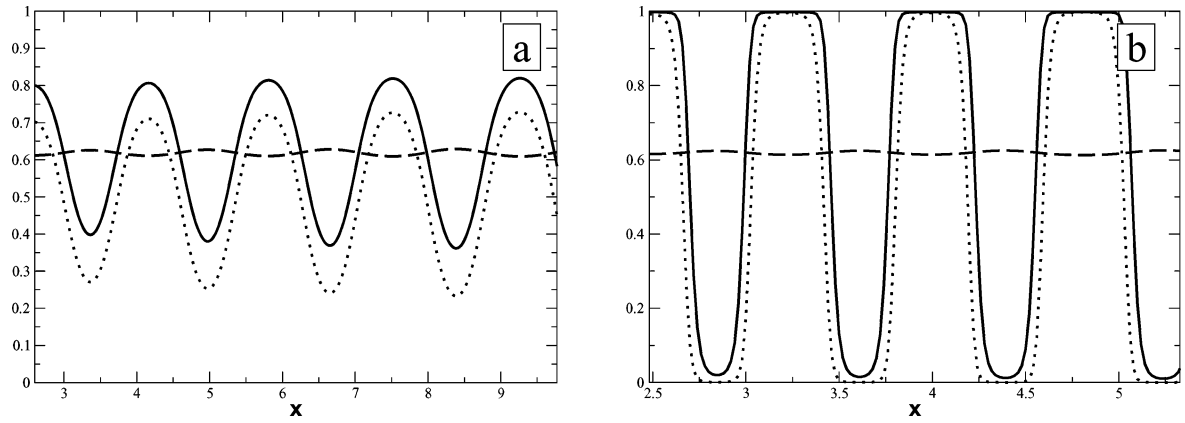

Figure 2. Stationary distribution profiles for species A (bold curve), B (dashed line), and C (dots) in a one-dimensional system in the case of attractive interactions with (a) $\epsilon = 5$ and (b) $\epsilon = 20$. Other parameters are the same as in Figure 1. Only part of the system with total size $L = 20$ is shown.

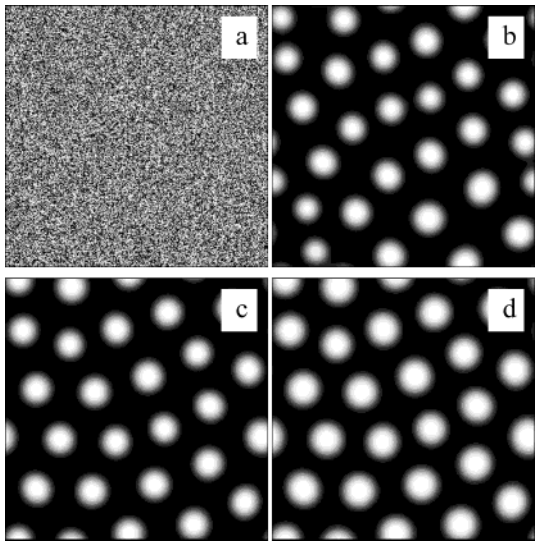

Figure 3. Development of the two-dimensional stationary pattern. Snapshots a, b, and c show spatial distributions of species A at time moments $t = 0$, 5, and 20, respectively. The snapshot d shows the spatial distribution of species C at $t = 20$. The linear size of the system is $L = 10$, and the parameters are the same as in Figure 1.

1 are chosen. Parts a, b, and c of Figure 3 display three subsequent snapshots of the coverage of species A. Figure 3d shows the spatial distribution of species *C* at a the same moment as in Figure 3c. Starting from a randomly perturbed uniform state (Figure 3a), the system develops a spatial pattern representing an array of dots. At an early evolution stage, the dots are different in sizes and their positions are less regular (Figure 3b). Later on, the dots become nearly identical and a hexagonal array is gradually formed (parts c and d of Figure 3). These dots represent islands where local coverages of species *A* and *C* are increased.

The presented patterns correspond to a relatively large interaction radius $r = 0.2$, which was chosen to clearly show the spatial variation inside interfaces. Analogous simulations were repeated for a smaller interaction radius of $r = 0.1$. The results are similar and therefore not displayed; the interfaces in the periodic domain pattern for strong attractive interactions become more narrow, as should be expected. We have furthermore compared the wavelength of the pattern, seen in numerical simulations, with the approximate analytical prediction (eq 28) yielded by the linear stability analysis in the limit of short-ranged interactions. For $r = 0.1$, the observed spatial period already agreed with this analytical prediction within several percent.

The instability of the uniform state is also found in numerical simulations in the case of repulsive interactions ($\epsilon < 0$). Parts a and b of Figure 4 display spatial profiles of all three species in the asymptotic stationary periodic patterns for relatively weak and strong repulsive interactions. The main difference with Figure 2 for attractive interactions is that now species A and C tend to avoid each other. The spatial segregation is almost complete in the case of strong repulsion (Figure 4b).

The numerical simulations, which have so far been presented, were performed assuming that $w = 0$. This means that the species C had no direct affect on the reaction rate and represented neither a promoter nor a poison. Next we demonstrate how these results are modified when $w \neq 0$.

Figure 5a shows spatial distributions of reactants and promoter in the periodic stationary pattern in the case of attractive interactions. Reaction enhancement inside mixed promoter−reactant domains leads to a decrease in the amplitude of the periodic pattern. In contrast to this, the amplitude is increased if species C is a poison (Figure 5b). If poisoning is sufficiently strong, the coverage of the second reactant *B* becomes also increased inside the domains, as already can be seen in Figure 5b.

If A and C repel each other, similar effects are observed; in the case of promotion, the reaction is most efficient in the domains filled with *C*, thus lowering the already small local coverage of *A* in these regions and leading to dense dots with stiff boundaries. Under strong promotion, the surface is decomposed into patches containing A surrounded by the poisoning species while the coverage in B is almost uniform. In the case of poisoning, the reaction is very weak inside the domains filled with C, which leads to a small increase of the coverage of A in these areas.

Compartmentalization of the catalytic surface, with one of the reactants concentrated in regularly spaced microscopic islands, can significantly influence the observed reactivity. To characterize this effect, we have numerically determined the actual reaction rate *R* per unit surface area under compartmentalization conditions and compared it with the computed reaction rate R_0 per unit area, assuming uniform distributions of all species. The quantity $\Delta R = (R - R_0)/R_0$ was then used to characterize the influence of compartmentalization.

Even when $w = 0$, so that species C is neither a promoter nor a poison, the formation of a periodic pattern has some effect on the reactivity. However, this effect is weak under such

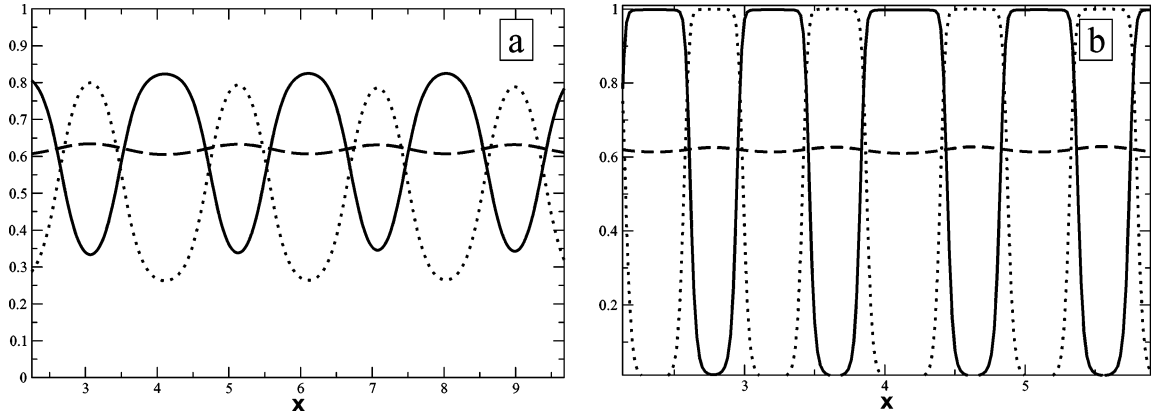

Figure 4. Stationary distribution profiles for species A (bold curve), B (dashed line), and C (dots) in a one-dimensional system in the case of repulsive interactions with (a) $\epsilon = -5$ and (b) $\epsilon = -20$. Other parameters are the same as in Figure 1.

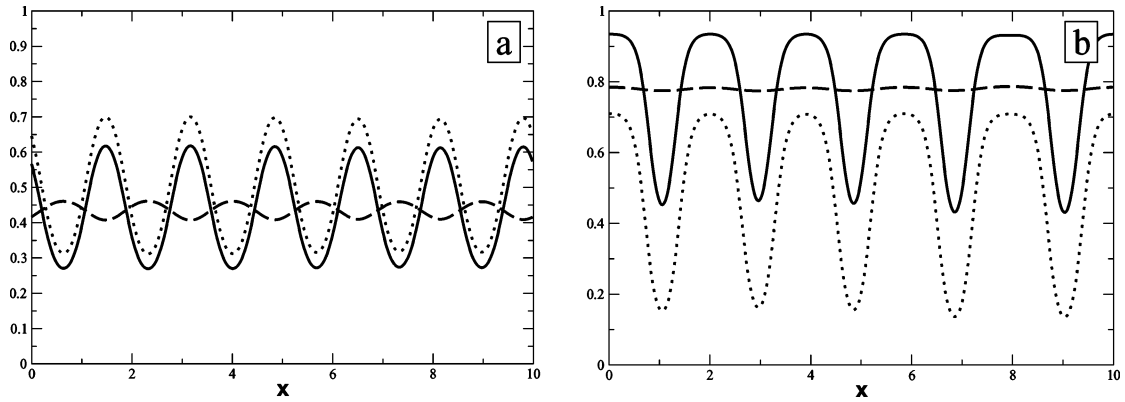

Figure 5. Stationary distribution profiles for species A (bold curve), B (dashed line), and C (dots) in a one-dimensional system (a) with a promoter ($w = 2$) and (b) with a poison ($w = -2$). Other parameters are the same as in Figure 1.

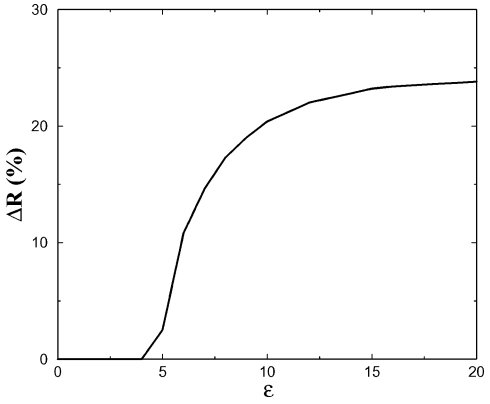

Figure 6. Growth of the relative global reaction rate under increase of the strength of attractive interactions for promoter with $w = 2$. Other parameters and system size are the same as in Figure 1.

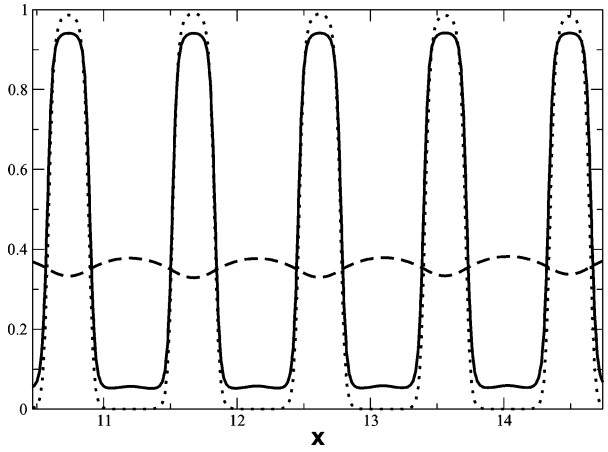

Figure 7. Stationary distribution profiles for reactants A (bold curve), B (dashed line), and promoter C (dots) in a one-dimensional system with $P_A = P_B = D_B = D_C = 1$, $D_A = 0.1$, $c = 0.3$, $r_0 = 0.2$, $\epsilon = 20$, and $w = 2$.

conditions, and only a decrease of ΔR by a few percents can be observed. The effect becomes much more pronounced when C is a promoter. Figure 6 shows the dependence of ΔR on the strength ϵ of attractive interactions in this situation. We see that the reactivity is substantially enhanced as ϵ grows and compartmentalization occurs. The maximum observed increase of the surface reactivity is about 25%.

When C is a poison, similar effects are observed. The global reaction rate is even lower than predicted in the homogeneous limit if A and C attract each other, since most A particles are then captured in dots with a high level of poison. If the interactions are repulsive, the global reaction rate is always smaller than its value without poisoning but can nevertheless become larger than predicted by the homogeneous evolution laws because adsorbate A is then principally located inside the domains which are poor in the poisoning species.

In the simulations, which we have so far shown, diffusion constants of all species were chosen equal ($D_A = D_B = D_C = 1$). Despite this, periodic patterns of surface concentrations have been found. This clearly indicates that such patterns are different in their origin from the Turing patterns, where a sufficiently strong difference of diffusion constants is always required. We have also performed some simulations where the diffusion constants were varied. It was observed that changes in the promoter diffusion constant D_C do not affect the final stationary pattern and only influence the transient process, which becomes

longer when diffusion of species C is slow. The independence of any stationary solution on the mobility of C is a general result, which follows directly from the model. Indeed, for a stationary pattern the left-hand side of eq 15 is zero and the coefficient D_C can be dropped out.

We have also verified that, as predicted by the linear stability analysis, spontaneous pattern formation is possible even at small promoter (or poison) concentrations c, if energetic interactions are strong enough. Moreover, such pattern formation was observed for different diffusion constants of the reactants A and B. As an example, Figure 6 shows a stationary pattern observed at a low mobility of the species A for a smaller concentation of the promoter C. In contrast to Figure 2a, the islands formed by species A have the same sizes as those of the species C. Between the islands, the concentration of A does not go to zero here and a certain level is maintained.

V. Discussion

By use of a simple model, we have shown that addition of promoter or poison species can destabilize the uniform state of surface chemical reactions. The instability leads to the development of a nonlinear stationary periodic pattern. For attractive interactions, the observed patterns represent arrays of dots, each dot being a mixed cluster of the promoter (or poison) and of the reactant attracted by the promoter species. If attraction is strong, the surface outside of the dots is depleted in this reactant and the reaction is concentrated within the dots which play a role of self-organized microreactors. This compartmentalization can affect the surface reactivity. By comparison of total reaction rates under mixed uniform conditions and in the presence of self-organized microstructures, a substantial enhancement of the promoter effect was found. Note that the effects of compartmentalization on chemical reactions in liquid solutions have recently been discussed.[25]

Catalytic reactions on microstructured surfaces, prefabricated using microlithography, have already been experimentally studied.[26] The principal result of our theoretical investigation is that the surface can also undergo spontaneous microstructuring through spatial redistribution of adsorbed atoms playing a role of promoters or poisons. In contrast to prefabricated patterns, such microstructures are flexible. They disappear when the reaction is switched off, and their properties can vary, adjusting to the reaction conditions. Taking into account that compartmentalization has a strong effect on the reaction rate, we note that nonequilibrium self-organization phenomena open a way to the construction of *adaptable* catalysts. Depending on the reaction parameters and external controls, such systems would be able to change their structure through redistribution of adsorbed metal atoms. Potentially, both reactivity and selectivity of a catalyst can thus be affected.

The aim of this theoretical study, employing a simple hypothetical reaction scheme, was merely to demonstrate the possibility of interesting nonlinear phenomena of nonequilibrium pattern formation in surface reactions with promoters or poisons. In the future, theoretical investigations should be extended to realistic models of various chemical reactions. Moreover, kinetic Monte Carlo simulations of such systems should also be performed, which would allow to take into account statistical fluctuations and lattice effects.

Acknowledgment. Financial support from the REACTOR program of European Science Foundation is acknowledged.

References and Notes

(1) Jakubith, S.; Rotermund, H. H.; Engel, W.; von Oertzen, A.; Ertl, G. *Phys. Rev. Lett*. **1990**, *65*, 3013.
(2) Mikhailov, A. S.; Ertl, G. *Chaos* **2002**, *12*, 1.
(3) Kiskinova, M. Poisoning and promotion in catalysis based on surface science concepts. In *Studies in Surface Science and Catalysis*; Delmon, B., Yates, J. T., Eds.; Elsevier: Amsterdam, 1992.
(4) Diehl, R. D.; McGrath, R. *Surf. Sci. Rep*. **1996**, *23*, 43.
(5) Marbach, H.; Günther, S.; Luersen, B.; Gregoratti, L.; Kiskinova, M.; Imbihl, R. *Catal. Lett.* **2002**, *83*, 161.
(6) Marbach, H.; Günther, S.; Gregoratti, L.; Kiskinova, M.; Imbihl, R. *Chem. Phys. Lett.* **2002**, *364*, 207.
(7) Marbach, H.; Lilienkamp, G.; Wei, H.; Günther, S.; Suchorski, Y.; Imbihl, R. *PCCP* **2003**, *5*, 2730.
(8) De Decker, Y.; Marbach, H.; Hinz, M.; Günther, S.; Kiskinova, M.; Mikhailov, A. S.; Imbihl, R. *Phys. Rev. Lett.* **2004**, *92*, 198305.
(9) Mikhailov, A. S.; Ertl, G. *Science* **1996**, *272*, 1596.
(10) Glotzer, S. C.; Di Marzio, E. A.; Muthukumar, M. *Phys. Rev. Lett*. **1995**, *74*, 2034.
(11) Tran-Cong, Q.; Harada, A. *Phys. Rev. Lett*. **1996**, *76*, 1162.
(12) Motoyama, M.; Ohta, T. *J. Phys. Soc. Jpn* **1997**, *66*, 2715.
(13) Tabe, Y.; Yokoyama, H. *Langmuir* **1995**, *11*, 4609.
(14) Reigada, R.; Sagues, F.; Mikhailov, A. S. *Phys. Rev. Lett*. **2002**, *89*, 038301.
(15) Hildebrand, M.; Mikhailov, A. S.; Ertl, G. *Phys. Rev. E* **1998**, *58*, 5483.
(16) Hildebrand, M.; Mikhailov, A. S.; Ertl, G. *Phys. Rev. Lett*. **1998**, *81*, 2602.
(17) Hildebrand, M.; Kuperman, M.; Wio, H.; Mikhailov, A. S.; Ertl, G. *Phys. Rev. Lett.* **1999**, *83*, 1475.
(18) Hildebrand, M.; Ipsen, M.; Mikhailov, A. S.; Ertl, G. *New J. Phys.* **2003**, *5*, 61.
(19) Mikhailov, A. S.; Ertl, G. *Chem. Phys. Lett.* **1995**, *238*, 104.
(20) Hildebrand, M.; Mikhailov, A. S. *J. Phys. Chem.* **1996**, *100*, 19089.
(21) Hildebrand, M.; Mikhailov, A. S. *J. Stat. Phys*. **2000**, *101*, 599.
(22) Vlachos, D. G.; Katsoulakis, M. A. *Phys. Rev. Lett.* **2000**, *85*, 3898.
(23) Katsoulakis, M. A.; Vlachos, D. G. *J. Chem. Phys.* **2003**, *119*, 9412.
(24) Mortensen, J. J.; Hammer, B.; Nørskov, J. K. *Surf. Sci.* **1998**, *414*, 315.
(25) Chavez, F.; Kapral, R. *Phys. Rev. E* **2002**, *65*, 056203.
(26) Li, X.; Kevrekidis, I. G.; Pollmann, M.; Papathanasiou, A. G.; Rotermund, H. H. *Chaos* **2002**, *12*, 190.